Cell Type-Specific Modulation of Layer 6A Excitatory Microcircuits by Acetylcholine in Rat Barrel Cortex

Danqing Yang[1], Robert Günter[2], Guanxiao Qi[1], Gabriele Radnikow[1] and Dirk Feldmeyer[1,3,4]*

[1]Institute of Neuroscience and Medicine, INM-10, Research Centre Jülich, D-52425 Jülich, Germany
[2]Institute of Neuroscience and Medicine, INM-2, Research Centre Jülich, D-52425 Jülich, Germany
[3]Department of Psychiatry, Psychotherapy and Psychosomatics, RWTH Aachen University, D-52074 Aachen, Germany.
[4]Jülich Aachen Research Alliance, Translational Brain Medicine (JARA Brain), D-52074 Aachen, Germany

*Corresponding author: Dirk Feldmeyer

Institute of Neuroscience and Medicine (INM-10) Research Centre Jülich D-52425 Jülich Germany

Tel.: +49-2461-61-5226

Fax: +49-2461-61-1778

E-mail: d.feldmeyer@fz-juelich.de

Abstract

Acetylcholine (ACh) is known to regulate cortical activity during different behavioral states, e.g. wakefulness and attention. Here we show a differential expression of muscarinic ACh receptors (mAChRs) and nicotinic AChRs (nAChRs) in different layer 6A (L6A) pyramidal cell (PC) types of somatosensory cortex. At low concentrations, ACh induced a persistent hyperpolarization in corticocortical (CC) but a depolarization in corticothalamic (CT) L6A PCs via M_4 and M_1 mAChRs, respectively. At ~1 mM ACh depolarized exclusively CT PCs via $\alpha_4\beta_2$ subunit-containing nAChRs without affecting CC PCs. Miniature EPSC frequency in CC PCs was decreased by ACh but increased in CT PCs. In synaptic connections with a presynaptic CC PC, glutamate release was suppressed via M_4 mAChR activation but enhanced by nAChRs via $\alpha_4\beta_2$ nAChRs when the presynaptic neuron was a CT PC. Thus, in layer 6A the interaction of mAChRs and nAChRs results in an altered excitability and synaptic release, effectively strengthening corticothalamic output while weakening corticocortical synaptic signaling.

Keywords: barrel cortex, layer 6, pyramidal cells, acetylcholine, muscarinic receptors, nicotinic receptors, corticocortical, corticothalamic

39 **Introduction**

40 Acetylcholine (ACh) has been shown to play a major role in memory processing, arousal, attention
41 and sensory signaling[1-7]. It has been demonstrated that the ACh concentration in the cerebrospinal
42 fluid increases during wakefulness and sustained attention[8,9]. In the neocortex release of ACh occurs
43 predominately via afferents originating from cholinergic neurons in the nucleus basalis of Meynert
44 of the basal forebrain[10-12]; their terminals are densely distributed throughout all neocortical layers[13-
45 15]. A classical view is that ACh invariably increases the excitability of excitatory neurons in
46 neocortex 16-20. However, a persistent hyperpolarization in layer 4 (L4) excitatory neurons was
47 found in somatosensory cortex[21,22]. This layer-specific cholinergic modulation may contribute to
48 improving the cortical signal-to-noise ratio[23-25].

49 Although extensive studies have been conducted on the cholinergic modulation of neocortical
50 excitatory neurons, the action of ACh on the layer 6 (L6) microcircuitry has not been systematically
51 investigated. Two main pyramidal cell (PC) classes exist in cortical layer 6, namely corticothalamic
52 (CT) and corticocortical (CC) PCs. These two neuron types differ in their axonal projection patterns,
53 dendritic morphological features, electrophysiological properties and expression of molecular
54 markers[26-30]. CC PCs have no subcortical target and send intracortical projections mainly within the
55 infra-granular layers[28]; CT PCs, in contrast, have few axons distributed in cortex and send
56 projections directly back to the thalamus thereby contributing to a feedback control of sensory
57 input[31-35]. The question how the function of these two classes of L6 PCs is modulated by ACh has
58 so far not been explored.

59 Recent optogenetic studies suggest that PCs in L5 and L6 receive direct cholinergic inputs[20,36]. In
60 these neurons, ACh induces a slowly desensitizing inward current in L6 PCs of prefrontal cortex
61 through activation of $\alpha_4\beta_2$ subunit containing synaptic nicotinic acetylcholine receptors
62 (nAChRs)[23,36-39]. However, there are very few studies focusing on the effects of muscarinic
63 acetylcholine receptors (mAChRs) in L6A neurons[29,40]. Here, using single and paired patch-clamp
64 recordings with simultaneous biocytin-filling, we investigated both muscarinic and nicotinic
65 modulation of morphologically identified excitatory neurons and their synaptic connections in
66 layer 6A of rat primary somatosensory barrel cortex. We found that ACh shows a cell type-specific
67 effect on both cellular and synaptic properties in L6A excitatory microcircuits through activation
68 of mAChRs and/or nAChRs. Our results reveal that two functionally and morphologically distinct
69 subpopulations of L6A PCs, CC and CT PCs, are differentially modulated by ACh. We

70 demonstrate that ACh suppresses intracortical synaptic transmission via somatodendritic
71 hyperpolarization and inhibition of presynaptic neurotransmitter release of CC PCs by activating
72 M_4Rs. In contrast, CT PC show a dual cholinergic modulation: These neurons are depolarized via
73 M_1 mAChRs and $\alpha_4\beta_2$ subunit-containing nAChRs while the presynaptic release probability is
74 enhanced by $\alpha_4\beta_2$nAChRs. In this way, ACh contributes to a facilitation of corticothalamic feedback.
75

76 ## Results

77 ### ACh either depolarizes or hyperpolarizes L6A PCs through activation of mAChRs

78 Whole-cell patch clamp recordings from L6A neurons were performed in acute brain slices of rat
79 barrel cortex with simultaneous biocytin fillings. During recordings, excitatory neurons were
80 distinguished from interneurons by their regular firing pattern with a low maximum firing
81 frequency. Following bath application of 100 μM ACh, one subset of L6A PCs showed a
82 membrane potential hyperpolarization by on average -2.0 ± 1.0 mV (n = 14), whereas another was
83 depolarized by +9.5 ± 6.1 mV (n = 15; **Fig. 1a**). In addition, 1 s current pulses were injected in the
84 recorded neuron to elicit AP firing before and during bath application of ACh. Under the supra-
85 threshold stimulus (100pA above the rheobase current), the firing frequency was decreased by ACh
86 in L6A PCs showing an ACh-induced hyperpolarization but increased in PCs that exhibit a
87 depolarizing ACh response (**Fig. 1a, b**). Notably, both ACh-induced hyperpolarization and
88 depolarization were not transient but persisted until the end of bath application. For L2/3 and L5
89 PCs it has been reported that the ACh-induced depolarization was preceeded by an initial transient
90 hyperpolarization mediated by 'small conductance', Ca^{2+}-activated K^+ channels[21,41-43]. We were able
91 to reproduce this finding under the same recording condition; however, the de- and hyperpolarizing
92 cholinergic response in L6A PCs induced by ACh puff application was always monophasic
93 (**Supplementary Fig. 1**).

94 To determine which fraction of the membrane potential changes in L6A pyramidal neurons is
95 mediated by mAChRs, 20 μM atropine (ATRO, a general mAChR antagonist) was applied in
96 voltage-clamp mode. Both the ACh-induced outward and inward currents were found to be strongly
97 blocked by ATRO (20 μM) **(Fig. 1 c, d)**, suggesting that both ACh response types in L6A excitatory
98 neurons are almost exclusively mediated by mAChRs. We hypothesized that the $G_{i/o}$ protein
99 coupled M_4 mAChR subtype (M_4Rs) mediates the hyperpolarizing effects while the $G_{q/11}$ protein-
100 coupled M_1 mAChR subtype (M_1Rs) is responsible for the depolarization induced by ACh
101 application. To test this, puff application of ACh (100 μM) was performed in the presence and
102 absence of the selective mAChR antagonists in the perfusion solution. In the presence of 1 μM
103 tropicamide (TRO, a selective M_4R antagonist), the ACh-induced hyperpolarization was abolished
104 (**Fig. 1e, g**). Conversely, the ACh-induced depolarization was blocked by 0.5 μM pirenzipine (PIR,
105 a selective M_1R antagonist; **Fig. 1f, h**). These results indicate that the persistent hyperpolarization

106 and depolarization induced by low concentrations of ACh are mediated exclusively by M_4Rs and
107 M_1Rs, respectively.

108 The dose-dependence of the muscarinic effects was investigated by bath application of increasing
109 concentrations of ACh in the presence of 1 µM mecamylamine (MEC, a general nAChR antagonist)
110 and 0.5 µM tetrodotoxin (TTX) (0.3 µM to 300 µM; **Fig. 1i, j**). The dose-response curve was
111 obtained by fitting the data to the Hill equation. For hyperpolarizing L6A PCs, the ACh
112 concentration for a half-maximum response (EC_{50}) was 6.2 ± 1.3 µM while for depolarizing neurons,
113 the EC_{50} was 26.7 ± 5.4 µM. Thus, an ACh concentration of 30 µM was adopted for all subsequent
114 experiments; this concentration resulted in a >50% of the maximum response in both subgroups of
115 L6A excitatory neurons. In addition, when only 30 µM ACh was used neurons did not respond
116 with AP firing which was occasionally observed when applying 100 µM ACh.

117

118 **Cholinergic responses in L6A PCs are cell-type specific**

119 To investigate whether the two different cholinergic response types are specific for a defined
120 L6A pyramidal cell type, we characterized L6A PCs by their morphological, electrophysiological
121 and molecular features. Here, a total of 105 excitatory L6A neurons were recorded and
122 morphologically reconstructed. Previous studies have consistently shown that CC and CT L6A
123 PCs can be distinguished reliably by their axonal projection patterns[26,27,30,44]. Of all excitatory cells,
124 74 (70.5%) were identified as putative CT PCs while 31 (29.5%) were putative CC PCs. CC L6A
125 PCs displayed a dense horizontal axonal projection pattern in infragranular layers spanning
126 several neighboring barrel columns; CT L6A PCs, on the other hand, showed a sparse columnar
127 axonal domain with the majority of collaterals projecting directly towards the pia and terminating
128 predominately in layer 4 **(cf Fig. 2a left and right panels**). CC PCs have a significantly larger
129 axonal (15523 ± 5013 µm vs. 5209 ± 1462 µm, $P < 0.001$) and dendritic length (5921 ± 1346 µm
130 vs. 5134 ± 1070 µm, $P < 0.05$) compared to CT PCs. Similar differences were also detected in the
131 horizontal axonal and dendritic field span (1714 ± 350 µm vs. 358 ± 111 µm, $P < 0.001$ and 361
132 ± 58 µm vs. 232 ± 28 µm, $P < 0.001$, respectively, for CC vs. CT L6A PCs). For CC L6A PCs
133 these values are likely to be strong underestimates (by ≥ 90%, cf.[45]) because in acute slice
134 preparations their long-range axonal collaterals will be severely truncated; however, this does not
135 prevent an unambiguous cell type identification. In addition, CC L6A PCs have more first order

136 axon collaterals ($p < 0.001$) but fewer dendrites ($p < 0.001$) than CT PCs **(Fig. 2b)**. The features
137 described above are reflected in the polar plots **(Fig. 2a)**.

138 In addition, we determined the electrophysiological properties of morphologically identified CC (n
139 = 11) and CT (n = 9) L6A PCs. Compared to CT PCs, CC PCs showed a significantly lower R_{in} (P
140 < 0.05), a longer onset time ($P < 0.01$) for the first action potential (AP) evoked by injecting a
141 rheobase current and a longer AP half-width ($P < 0.05$). Trains of spikes were elicited to examine
142 the firing behavior. The AP adaptation ratio (2nd ISI/10th ISI) of CC PCs was smaller ($P < 0.05$) than
143 that of CT cells because they exhibited an initial spike burst. **(Supplementary Fig. 2).** The
144 differences in passive and active electrophysiological properties found here are in accordance with
145 previous studies[26,40].

146 Furthermore, the nuclear transcription factor Fork-head box protein P2 (FoxP2) is co-expressed
147 with the neurotensin receptor 1 (NtsR1) gene, a molecular marker for CT L6A PCs in mice[29,46]. To
148 identify the expression of FoxP2 in L6A PCs, we performed whole-cell recordings with
149 simultaneous filling of biocytin and fluorescent Alexa Fluor® 594 dye (n = 14). Subsequently,
150 brain slices were processed for FoxP2 immunofluorescence staining. We found that CT L6A PCs
151 were FoxP2-positive while CC PCs are FoxP2-negative **(Supplementary Fig. 3a,b)**. The tight
152 correlation between neuronal morphology, electrophysiology and FoxP2 expression demonstrates
153 the reliability of classification based on axonal projection patterns of CC and CT PCs.

154 ACh at a concentration of 30 µM was bath-applied to 63 morphological identified L6A neurons.
155 CC L6A PCs showed a hyperpolarizing response with a mean amplitude of -1.76 ± 4.28 mV (from
156 -61.9 ± 5.6 mV to -63.6 ± 7.0 mV, $P < 0.05$, n = 35). In contrast, ACh (30 µM) induced a strong
157 depolarization with a mean amplitude of +11.4 ± 4.6 mV (from -70.3 ± 5.1 mV to -58.8 ± 7.4 mV,
158 $P < 0.001$, n = 14) in CT PCs without exception (**Fig. 2c)**. In **Fig. 2d**, ACh-induced membrane
159 potential changes are plotted against the horizontal axonal field span revealing a strong correlation
160 between axonal morphology and cholinergic response for the two L6A pyramidal cell types. In
161 addition, by performing immunostaining we confirmed that M_4Rs were enriched within L6A. We
162 found that M_4R-positive neurons were FoxP2-negative while virtually no FoxP2-positive neuron
163 expressed M_4Rs **(Supplementary Fig. 3d)**. This is consistent with our pharmacological result that
164 only FoxP2-negative CC PCs showed a M_4Rs-mediated hyperpolarization following ACh
165 application **(Supplementary Fig. 3)**.

166

167 **CT PCs are selectively activated by high concentrations of ACh via α4β2 nAChRs**

168 As demonstrated above, the depolarizing and hyperpolarizing effects of ACh in L6A PCs can be
169 attributed to the activation of M_1 and M_4 mAChRs, respectively (**Fig. 1c, d**). However, previous
170 studies have shown that ACh excites L6A excitatory neurons by activating nAChRs[23,36,37,39]. In order
171 to investigate the functional role of nAChRs in L6A of rat barrel cortex, we perfused slices
172 continuously with 200 nM ATRO. Under this condition, 30 μM ACh had no effect on both CC and
173 CT PCs ($P > 0.05$ for CC cells, $n = 5$; $P > 0.05$ for CT cells, $n = 5$) (**Fig. 3a**); application of 1 mM
174 ACh, however, strongly depolarized CT PCs ($P < 0.001$, $n = 12$) while CC PCs showed no response
175 ($P > 0.05$, $n = 4$; **Fig. 3b**). Our results demonstrate that both the muscarinic and nicotinic
176 modulation of L6A PCs is cell-type specific; nAChRs are present solely in CT L6A PCs and
177 activated substantially only by high ACh concentrations. To determine the concentration range in
178 which ACh activates postsynaptic nAChRs, we measured the dose-response curve for ACh in the
179 presence of 200 nM ATRO. A fit of dose-response relationship to the Hill equation gave an EC_{50}
180 of 1.2 ± 0.3 mM ($n = 5$) for the nicotinic ACh response (**Fig. 3c**), a value more than about two orders
181 of magnitude larger than those of the de- and hyperpolarizing muscarinic response.

182 It has been reported that the expression of nAChR subtypes in the neocortex exhibits layer-
183 specificity. L6A PCs in prefrontal cortex show a slow inward current to ACh by activating nAChRs
184 containing the α_4 and β_2 subunits[23,36]. To confirm that this nAChR subtype mediates the response,
185 the response of CT L6A PCs to application of 1 mM ACh was recorded in an ATRO-containing
186 perfusion solution. In the presence of DHßE (10 μM), a nicotinic antagonist specific for $\alpha_4\beta_2$
187 nAChRs, the ACh-dependent depolarization in CT PCs was eliminated, suggesting that CT L6A
188 PCs express postsynaptic $\alpha_4\beta_2$ subunit-containing nAChRs (**Fig. 3d**).

189

190 **ACh differentially modulate miniature spontaneous activity of CC and CT L6A PCs**

191 In addition to changing the membrane properties and excitability of neurons, ACh is also a
192 powerful modulator of neurotransmitter release. Therefore, we measured the amplitude and
193 frequency of miniature spontaneous activity by performing whole-cell voltage-clamp recordings
194 from L6A PCs. The membrane potential was held at -70 mV and inward miniature EPSCs
195 (mEPSCs) were recorded in the presence of TTX (0.5 μM) and gabazine (10 μM).

196 We found that ACh differentially modulates miniature spontaneous activity in both L6A CC and
197 CT PCs. The frequency but not the amplitude of mEPSCs in CC L6A PCs was significantly

198 decreased by application of 30 µM ACh (2.8 ± 0.8 vs. 2.2 ± 1.0 Hz; n = 7, P < 0.01), an effect that
199 was blocked by the M_4Rs antagonist tropicamide (2.2 ± 1.0 vs. 2.8 ± 1.0 Hz; n = 7, P < 0.01) (**Fig.**
200 **4a-c**). This suggests that ACh decreases the neurotransmitter release probability at synapses with
201 CC L6A PCs via presynaptic M_4Rs. Similarly, when DHßE was co-applied with tropicamide and
202 ACh, a reduction of mEPSC frequency without a change in mEPSC amplitude was observed
203 (**Supplementary Fig. 4**). This implies that in addition to M_4Rs, $\alpha_4\beta_2$ nAChRs also play a role in
204 the cholinergic modulation of excitatory synaptic transmission onto CC PCs.

205 In contrast to CC L6A PCs, application of 30 µM ACh significantly decreased the inter-event
206 interval of mEPSCs in CT PCs, reflecting an increase in mEPSC frequency (0.95 ± 0.36 vs. 2.12 ±
207 0.68 Hz; n = 7, P < 0.01) while the mEPSc amplitude remained unaffected. Because ATRO did not
208 affect the mEPSC frequency, we argued that the cholinergic effects on spontaneous mEPSCs in
209 CT L6A PCs were not mediated by mAChRs but exclusively by presynaptic nAChRs. To test this,
210 10 µM DHßE was co-applied with ACh. In the presence of DHßE, the ACh-induced increase of
211 mEPSCs frequency in CT L6A PCs was reduced to control level (2.12 ± 0.68 vs. 1.01 ± 0.55; n =
212 7, P < 0.05; **Fig. 4d-f**). These results suggest that ACh potentiates excitatory synaptic transmission
213 onto L6A CT PCs exclusively via presynaptic $\alpha_4\beta_2$ subunit containing nAChRs.

214

215 **ACh induces a reduction of presynaptic neurotransmitter release in CC L6A PCs but an an**
216 **increase in CT PCs**

217 To elucidate cholinergic effects on L6A PCs at pre- and postsynaptic sites independently, paired
218 recordings and simultaneous biocytin fillings of synaptically coupled L6A neurons were performed.
219 Excitatory neurons were classified as either CT and CC PCs based on the criteria mentioned above.
220 During recordings, inhibitory interneurons were preliminarily identified by their high frequency
221 AP firing pattern. After reconstructions, interneurons were further distinguished based on
222 morphological features such as lack of dendritic spines. 34 excitatory connections were established
223 by presynaptic CC PCs. We found that ACh suppresses the synaptic efficacy of neuronal
224 connections established by presynaptic CC PCs regardless of the postsynaptic neuron type **(Fig. 5)**.
225 The unitary EPSP (uEPSP) amplitude of all synaptic connections with a presynaptic L6A CC PC
226 were all significantly decreased by ACh (30 µM). For CC-CC connections the uEPSP amplitude
227 decreased from 0.45 ± 0.32 mV to 0.19 ± 0.14 mV (n = 20 pairs, P < 0.001) and for CC-CT
228 connections changed from 0.35 ± 0.22 mV to 0.19 ± 0.13 mV (n = 5 pairs, P < 0.05). For CC-

229 interneuron connections the mean uEPSP was reduced from 0.90 ± 0.90 mV to 0.52 ± 0.58 mV (n
230 = 9 pairs, $P < 0.05$) in the presence of ACh. ACh also significantly increased the paired-pulse ratio
231 (PPR) of CC-CC (1.0 ± 0.4 vs. 1.5 ± 0.7, $P < 0.01$), CC-CT (1.2 ± 0.7 vs. 2.1 ± 1.6, $P < 0.05$) and
232 CC-interneuron (1.0 ± 0.5 vs. 1.2 ± 0.5, $P < 0.01$) connections. Following ACh application, CC-
233 CC connections and CC-interneuron connections showed an increase in the CV; at CC-interneuron
234 connections the failure rate was also significantly increased **(Fig. 5 e; Supplementary Tab. 1)**.
235 These changes in the EPSP properties suggest that ACh decreases the neurotransmitter release
236 probability of intra-laminar connections established by a presynaptic L6A CC PC. Other synaptic
237 properties, like rise time, latency and decay time, were not affected by ACh **(Supplementary Tab.**
238 **1)**.

239 Previous studies have shown that ACh may inhibits intracortical excitatory synaptic transmission
240 at some synaptic connections through activation of presynaptic M_4 mAChRs[21,47,48]. To test whether
241 the ACh-induced suppression of the efficacy of synaptic connections with a presynaptic CC L6A
242 PC is mediated by M_4 mAChR activation, 1 μM TRO (a selective antagonist of M_4Rs) was co-
243 applied with ACh (30 μM) after bath application of ACh alone. The effects of ACh on synaptic
244 connections established by CC PCs (n = 6 pairs, comprising 2 CC-CC, 1 CC-CT and 3 CC-
245 interneuron connections) were completely blocked by TRO. The EPSP amplitude decreased from
246 1.0 ± 0.8 mV to 0.3 ± 0.2 mV during ACh application and fully recovered to 1.0 ± 0.8 mV during
247 co-application of ACh and TRO. Moreover, TRO also blocked the ACh effects on the CV (0.8 ±
248 0.2 for control vs. 0.9 ± 0.3 for ACh and TRO; n = 6 pairs, $P = 0.75$) and failure rate (27.0 ±
249 17.6 % for control vs. 26.3 ± 19.6 % for ACh and TRO; n = 6 pairs, $P = 1.00$) **(Fig. 6)**. In
250 addition to reversing the ACh-induced increase in the PPR, TRO increased the PPR of
251 connections established by CC PCs. Co-application of ACh and TRO resulted in a smaller PPR
252 compared to control (1.1 ± 0.3 vs. 1.3 ± 0.4; n = 6 pairs, $P < 0.05$) **(Fig. 6)**. In order to isolate the
253 presynaptic effect of ACh on L6A intra-laminar connections established by presynaptic CC PCs,
254 a CC-CT synaptically coupled pair was recorded. The ACh-induced reduction in synaptic release
255 probability recovered only after co-application of TRO together with PIR but not when PIR (0.5
256 μM) was applied alone **(Supplementary Fig. 5)**.

257 Because of their sparse and narrow axonal domain, L6A CT PCs rarely innervate neurons in their
258 home layer and their intracortical synaptic connections are remarkably weak and unreliable[44,49,50].
259 Here we applied ACh (30 μM) to seven synaptic connections established by a presynaptic CT PC
260 in L6A, including two CT-CT, one CT-CC and four CT-interneuron connections. In all synaptic

261 connections established by CT PCs ACh significantly enhanced the EPSP amplitude (0.10 ± 0.08
262 mV vs. 0.15 ± 0.10 mV; n = 7 pairs, $P < 0.05$) and reduced the PPR (3.0 ± 1.7 vs. 0.8 ± 0.6; n = 7
263 pairs, $P < 0.05$) **(Fig. 7)**. The ACh-mediated reduction in the PPR suggests a presynaptic locus for
264 synaptic modulation. Because these connections display very small unitary EPSP amplitudes and
265 frequent failures, the signal-to-noise ratio was often too low to appropriately calculate the CV and
266 failure rate. No significant differences were detected in rise time, decay time and latency
267 **(Supplementary Tab. 1)**. Our findings indicate that in contrast to the inhibition of presynaptic
268 release in L6A CC PCs, ACh enhances the synaptic efficacy of the weak connections established
269 by a presynaptic CT PC.

270 To determine the AChR subtype that mediates the increase in synaptic efficacy at these connections,
271 we tested whether the selective antagonists of the M_1Rs (PIR), homomeric the α_7 subunit-containing
272 nAChRs (methyllycaconitine, MLA) and the heteromeric $\alpha_4ß_2$ subunit-containing nAChRs (DHßE)
273 could block the effect of ACh on synaptic connections with a presynaptic CT PC. While PIR and
274 MLA had no effect, DHßE blocked the increase of EPSP amplitude and decrease of PPR **(Fig. 8)**.
275 This indicates that the ACh-induced enhancement of synaptic efficacy is induced by activation of
276 $\alpha_4ß_2$ subunit-containing nAChRs in presynaptic CT PCs.

277

278 **Discussion**

279 We investigated the cholinergic modulation of CT and CC PCs in layer 6A of the barrel cortex.
280 We showed that (i) low concentrations of ACh differentially modulate the L6A microcircuitry by
281 persistently depolarizing CT but hyperpolarizing CC L6A PCs. These effects are monophasic and
282 mediated via M_1 and M_4 mAChRs, respectively; (ii) a nicotinic ACh response was observed
283 exclusively in CT PCs only when a high ACh concentration was applied. In addition, (iii) low
284 concentrations of ACh increases the frequency of miniature EPSCs via presynaptic nAChRs in
285 L6A CT but decreases that of CC PCs via M_4Rs. To better understand the effects of ACh on
286 intralaminar synaptic transmission, recordings were performed from synaptically coupled L6A PC
287 pairs. We found that (iv) in neuronal connections with a presynaptic CC PC the neurotransmitter
288 release probability was reduced via activation of M_4Rs but (v) increased in connections with a
289 presynaptic CT L6A neuron by $\alpha_4\beta_2$ nAChR activation. Our results reveal that two functionally and
290 morphologically distinct subpopulations of L6A PCs are affected differentially by ACh acting on
291 both mAChRs and nAChRs.

292

293 **Synergistic modulation of L6A PCs by mAChRs and nAChRs**

294 In a number of studies investigating the nAChR response of L6 PCs in different cortical areas only
295 high ACh concentration (≥ 1 mM) have been applied because the ACh affinity of nAChRs is
296 substantially lower than that of mAChRs[23,36,37,39]. Under this condition any mAChR effect is almost
297 entirely masked by the strong nicotinic response so that any involvement of mAChRs has been
298 explicitly ruled out. Here we demonstrate for the first time that mAChRs play crucial roles in both
299 pre- and postsynaptic modulation of L6A PC activity. Both the pre- and postsynaptic effects of
300 mAChRs are already present at low ACh concentrations (1-10 μM) suggesting that
301 neuromodulation via mAChRs is tonically present and mediated by volume transmission[51,52]. On the
302 other hand, only a high concentration of ACh (EC_{50} of ~1 mM) could effectively depolarize CT
303 L6A PCs via nAChRs, but an up-regulation of presynaptic vesicle release via $\alpha_4\beta_2$ subunit-
304 containing nAChRs was already observed in the presence of 30 μM ACh. This $\alpha_4\beta_2$ nAChR-
305 mediated effect was found for spontaneous excitatory synaptic activity as well as for CT-formed
306 monosynaptic connections, suggesting that presynaptic nAChR are expressed on synaptic boutons
307 of both CT L6A axons and other glutamatergic afferents (e.g. from thalamus or other cortical
308 regions). Single channel currents from nAChRs can be activated already by low concentrations of

309 ACh[53,54]. Because of the electrotonic compact structure of a presynaptic bouton even the opening of
310 a few nAChR receptor channels may result in a depolarisation that is sufficiently strong to increase
311 the open probability of presynaptic Ca^{2+} channels and hence the neurotransmitter release.

312 Furthermore, in some L6 PCs the α_5 nAChR subunit co-assembles with the α_4 and $ß_2$ subunits[23,36].
313 Nicotinic AChRs containing the α_4, $ß_2$ and α_5 subunits have a higher Ca^{2+} permeability than those
314 composed of α_4 and $ß_2$ nAChR subunits alone[55]. In the presynaptic terminals, Ca^{2+} entry via $\alpha_4ß_2\alpha_5$
315 nAChRs into the presynaptic bouton could enhance neurotransmitter release provided these
316 channels are located sufficiently close to the release site.

317

318 **Cholinergic activation by endogenous ACh in neocortical L6**

319 In the cortex, ACh levels change dramatically during different stages of waking and sleep[8,9]. It has
320 been suggested that high ACh levels serve to enhance the response to sensory stimuli by increasing
321 the strength of afferent input while low concentration of ACh contributes in the consolidation of
322 encoded information[56]. Cholinergic signalling has been described to occur via a volume release
323 mechanism[52], which is slow and unspecific. Volume release of ACh reaches concentrations in a low
324 micromolar range, spreads widely over neocortical layers and activates predominantly mAChRs.
325 In addition, cholinergic synapses have been identified particularly in deep layers of neocortex and
326 less so in superficial cortical layers[20,36,57]. At these cholinergic synapses, ACh reaches a high
327 concentration in the synaptic cleft, thereby activating postsynaptic nAChRs in L6 PCs[36]. Because
328 cholinergic synapses in the neocortex are small[58], ACh released into the synaptic cleft may spill
329 over into the perisynaptic space. Subsequently, the extra-synaptic AChRs on presynaptic boutons
330 of CT PCs are activated resulting in an increase of release probability (**Fig. 7**). Thus, nAChRs and
331 mAChRs act on different time scales and at different neurotransmitter concentrations, resulting in
332 a striking complexity of the cholinergic modulation of neocortical signaling.

333

334 **The cell type-specific effect of ACh in L6A**

335 ACh has been shown to induce a persistent depolarization of L2/3 and L5 PCs but a
336 hyperpolarization of excitatory L4 neurons[21,43,59]. Here, we demonstrate that ACh modulates PCs not
337 only in a layer-specific but also a cell type-specific way that can be attributed to a cell type-
338 dependent expression of mAChRs (**Fig. 9**). In L6A of barrel cortex, ACh hyperpolarizes CC PCs
339 but depolarizes CT PCs via activation of M_4Rs and M_1Rs, respectively. The action potential firing

340 frequency was decreased by ACh in CC PCs but increased in CT PCs, thereby modulating the
341 excitability and signal propagation in L6A PCs in a cell-specific manner. In addition, CT L6A PCs
342 but not CC PCs showed a strong $\alpha_4\beta_2$ nAChR-mediated response (**Fig. 9**). This is consistent with
343 previous findings in L6 of prefrontal cortex that regular spiking neurons have a larger nicotinic
344 receptor-mediated inward current following ACh application when compared with bursting
345 neurons[37]. A cell type-specific neuromodulation was also discovered previously in deep layers of
346 medial prefrontal cortex for neuromodulators such as noradrenaline, dopamine and adenosine[60-64].

347 By studying miniature spontaneous activity of L6A CC and CT PCs, we found that ACh both
348 increases the excitatory synaptic release onto CC and CT PCs by activation of $\alpha_4\beta_2$ nAChRs (**Fig.**
349 **9**). Because CT PCs express $\alpha_4\beta_2$ nAChRs, an increase in spontaneous activity may result from the
350 enhanced release probability at CT L6 PC boutons; however, the intracortical axon density of these
351 PCs is low so that their contribution to the spontaneous mEPSC frequency is minimal. On the other
352 hand, activation of nAChRs increases thalamocortical transmission onto L3, L4 and L5 neocortical
353 neurons[47,65,66]. Thus, the increased excitatory transmission onto L6A PCs is probably resulting to a
354 large degree from a higher release probability at thalamocortical and less so from intracortical
355 synapses. In addition, CC PCs receive more intra-laminar inputs than CT PCs, which can be
356 suppressed by ACh via M_4Rs. Therefore, the ACh-induced reduction of mEPSC frequency in CC
357 PCs could be a combinatorial effect on thalamocortical and intracortical transmission.

358 It has been proposed that ACh increases the signal-to-noise ratio (SNR) of sensory signaling by
359 selectively enhancing thalamocortical inputs over intracortical synaptic transmission[47,67,68]. ACh has
360 been found to suppress the efficacy of excitatory intracortical connections in different layers
361 including L2/3, L4 and L5[21,47,48]. Here, a differential cholinergic modulation of presynaptic
362 neurotransmitter release was observed in CC and CT L6A PC types. ACh suppresses synaptic
363 transmission in excitatory L6A connections with presynaptic CC PCs through activation of M_4Rs
364 but potentiates connections with a presynaptic CT PCs via presynaptic $\alpha_4\beta_2$ nAChRs (**Fig. 9**); no α_7
365 nAChR or M_1R effect on synaptic transmission was observed.

366 In hippocampus and some subcortical structures such as the ventral tegmental area, glutamatergic
367 synapses are known to be facilitated by nAChRs located on presynaptic terminals[69,70]. However,
368 very few studies demonstrate an ACh-mediated enhancement of intracortical excitatory synaptic
369 transmission. Recently, it has been shown that excitatory synaptic transmission between PCs and
370 somatostatin-positive interneurons in layer 2 of mouse barrel cortex is increased by ACh via

activating nAChRs[71]. Although an increase of synaptic efficacy was observed in connections with a presynaptic CT PCs, this type of synaptic connections are rare, generally weak and very unreliable[49,50]. Therefore we propose that ACh mainly acts on CT PCs not primarily by increasing intracortical synaptic transmission but rather by facilitating corticothalamocortical feedback; this facilitation will occur already at ACh levels in the low micromolar range.

Acknowledgement

We thank Werner Hucko for excellent technical assistance and Dr. Dr. Karlijn van Aerde for custom-written macros in Igor Pro software. We warmly thank Dr. Chao Ding for helpful discussions and Dr. Vishalini Emmenegger for proofreading the manuscript.

Funding

This work was supported by the Helmholtz Society, the DFG Research Group - BaCoFun (grant no. Fe471/4-2 to D.F.), the European Union's Horizon 2020 Research, Innovation Programme under Grant Agreement No. 785907 (HBP SGA2; to DF) and the China Scholarship Council (to D.Y.).

Author contributions

D.F., G.R. and D.Y. designed the research; D.Y., R.G. and G.Q. performed experiments and data analysis; D.Y., D.F. and G.R. wrote the manuscript. The authors declare no conflicts of interest.

391 ## References

392 1 Jones, B. E. Activity, modulation and role of basal forebrain cholinergic neurons innervating the cerebral
393 cortex. *Prog Brain Res* **145**, 157-169, doi:10.1016/S0079-6123(03)45011-5 (2004).

394 2 Hasselmo, M. E. The role of acetylcholine in learning and memory. *Curr Opin Neurobiol* **16**, 710-715,
395 doi:10.1016/j.conb.2006.09.002 (2006).

396 3 Herrero, J. L. *et al.* Acetylcholine contributes through muscarinic receptors to attentional modulation in
397 V1. *Nature* **454**, 1110-1114, doi:nature07141 [pii] 10.1038/nature07141 (2008).

398 4 Hasselmo, M. E. & Sarter, M. Modes and models of forebrain cholinergic neuromodulation of cognition.
399 *Neuropsychopharmacology* **36**, 52-73, doi:10.1038/npp.2010.104 (2011).

400 5 Thiele, A. Muscarinic signaling in the brain. *Annu Rev Neurosci* **36**, 271-294, doi:10.1146/annurev-
401 neuro-062012-170433 (2013).

402 6 Wester, J. C. & Contreras, D. Differential modulation of spontaneous and evoked thalamocortical
403 network activity by acetylcholine level in vitro. *J Neurosci* **33**, 17951-17966,
404 doi:10.1523/JNEUROSCI.1644-13.2013 (2013).

405 7 Ma, S., Hangya, B., Leonard, C. S., Wisden, W. & Gundlach, A. L. Dual-transmitter systems regulating
406 arousal, attention, learning and memory. *Neurosci Biobehav Rev* **85**, 21-33,
407 doi:10.1016/j.neubiorev.2017.07.009 (2018).

408 8 Himmelheber, A. M., Sarter, M. & Bruno, J. P. Increases in cortical acetylcholine release during
409 sustained attention performance in rats. *Brain Res Cogn Brain Res* **9**, 313-325 (2000).

410 9 Teles-Grilo Ruivo, L. M. *et al.* Coordinated Acetylcholine Release in Prefrontal Cortex and
411 Hippocampus Is Associated with Arousal and Reward on Distinct Timescales. *Cell Rep* **18**, 905-917,
412 doi:10.1016/j.celrep.2016.12.085 (2017).

413 10 Mesulam, M. M., Mufson, E. J., Wainer, B. H. & Levey, A. I. Central cholinergic pathways in the rat:
414 an overview based on an alternative nomenclature (Ch1-Ch6). *Neuroscience* **10**, 1185-1201 (1983).

415 11 Zaborszky, L. *et al.* Neurons in the basal forebrain project to the cortex in a complex topographic
416 organization that reflects corticocortical connectivity patterns: an experimental study based on retrograde
417 tracing and 3D reconstruction. *Cereb Cortex* **25**, 118-137, doi:10.1093/cercor/bht210 (2015).

418 12 Paul, S., Jeon, W. K., Bizon, J. L. & Han, J. S. Interaction of basal forebrain cholinergic neurons with
419 the glucocorticoid system in stress regulation and cognitive impairment. *Front Aging Neurosci* **7**, 43,
420 doi:10.3389/fnagi.2015.00043 (2015).

421 13 Eckenstein, F. P., Baughman, R. W. & Quinn, J. An anatomical study of cholinergic innervation in rat
422 cerebral cortex. *Neuroscience* **25**, 457-474 (1988).

14 Henny, P. & Jones, B. E. Projections from basal forebrain to prefrontal cortex comprise cholinergic, GABAergic and glutamatergic inputs to pyramidal cells or interneurons. *Eur J Neurosci* **27**, 654-670, doi:10.1111/j.1460-9568.2008.06029.x (2008).

15 Kalmbach, A., Hedrick, T. & Waters, J. Selective optogenetic stimulation of cholinergic axons in neocortex. *J Neurophysiol* **107**, 2008-2019, doi:10.1152/jn.00870.2011 (2012).

16 McCormick, D. A. & Prince, D. A. Two types of muscarinic response to acetylcholine in mammalian cortical neurons. *Proc Natl Acad Sci U S A* **82**, 6344-6348, doi:10.1073/pnas.82.18.6344 (1985).

17 Mednikova, Y. S., Karnup, S. V. & Loseva, E. V. Cholinergic excitation of dendrites in neocortical neurons. *Neuroscience* **87**, 783-796 (1998).

18 Desai, N. S. & Walcott, E. C. Synaptic bombardment modulates muscarinic effects in forelimb motor cortex. *J Neurosci* **26**, 2215-2226, doi:10.1523/JNEUROSCI.4310-05.2006 (2006).

19 Zhang, Z. & Seguela, P. Metabotropic induction of persistent activity in layers II/III of anterior cingulate cortex. *Cereb Cortex* **20**, 2948-2957, doi:10.1093/cercor/bhq043 (2010).

20 Hedrick, T. & Waters, J. Acetylcholine excites neocortical pyramidal neurons via nicotinic receptors. *J Neurophysiol* **113**, 2195-2209, doi:10.1152/jn.00716.2014 (2015).

21 Eggermann, E. & Feldmeyer, D. Cholinergic filtering in the recurrent excitatory microcircuit of cortical layer 4. *Proc Natl Acad Sci U S A* **106**, 11753-11758, doi:10.1073/pnas.0810062106 (2009).

22 Dasgupta, R., Seibt, F. & Beierlein, M. Synaptic Release of Acetylcholine Rapidly Suppresses Cortical Activity by Recruiting Muscarinic Receptors in Layer 4. *J Neurosci* **38**, 5338-5350, doi:10.1523/JNEUROSCI.0566-18.2018 (2018).

23 Poorthuis, R. B. *et al.* Layer-specific modulation of the prefrontal cortex by nicotinic acetylcholine receptors. *Cereb Cortex* **23**, 148-161, doi:10.1093/cercor/bhr390 (2013).

24 Obermayer, J., Verhoog, M. B., Luchicchi, A. & Mansvelder, H. D. Cholinergic Modulation of Cortical Microcircuits Is Layer-Specific: Evidence from Rodent, Monkey and Human Brain. *Front Neural Circuits* **11**, 100, doi:10.3389/fncir.2017.00100 (2017).

25 Radnikow, G. & Feldmeyer, D. Layer- and Cell Type-Specific Modulation of Excitatory Neuronal Activity in the Neocortex. *Front Neuroanat* **12**, 1, doi:10.3389/fnana.2018.00001 (2018).

26 Kumar, P. & Ohana, O. Inter- and intralaminar subcircuits of excitatory and inhibitory neurons in layer 6a of the rat barrel cortex. *J Neurophysiol* **100**, 1909-1922, doi:10.1152/jn.90684.2008 (2008).

27 Zhang, Z. W. & Deschenes, M. Intracortical axonal projections of lamina VI cells of the primary somatosensory cortex in the rat: a single-cell labeling study. *J Neurosci* **17**, 6365-6379 (1997).

28 Thomson, A. M. Neocortical layer 6, a review. *Front Neuroanat* **4**, 13, doi:10.3389/fnana.2010.00013 (2010).

456 29 Sundberg, S. C., Lindstrom, S. H., Sanchez, G. M. & Granseth, B. Cre-expressing neurons in visual
457 cortex of Ntsr1-Cre GN220 mice are corticothalamic and are depolarized by acetylcholine. *J Comp*
458 *Neurol* **526**, 120-132, doi:10.1002/cne.24323 (2018).

459 30 Pichon, F., Nikonenko, I., Kraftsik, R. & Welker, E. Intracortical connectivity of layer VI pyramidal
460 neurons in the somatosensory cortex of normal and barrelless mice. *Eur J Neurosci* **35**, 855-869,
461 doi:10.1111/j.1460-9568.2012.08011.x (2012).

462 31 Beierlein, M. & Connors, B. W. Short-term dynamics of thalamocortical and intracortical synapses onto
463 layer 6 neurons in neocortex. *J Neurophysiol* **88**, 1924-1932 (2002).

464 32 Yang, Q. *et al.* Intrinsic properties of and thalamocortical inputs onto identified corticothalamic-VPM
465 neurons. *Somatosens Mot Res* **31**, 78-93, doi:10.3109/08990220.2013.869495 (2014).

466 33 Oberlaender, M. *et al.* Cell type-specific three-dimensional structure of thalamocortical circuits in a
467 column of rat vibrissal cortex. *Cereb Cortex* **22**, 2375-2391, doi:10.1093/cercor/bhr317 (2012).

468 34 Constantinople, C. M. & Bruno, R. M. Deep cortical layers are activated directly by thalamus. *Science*
469 **340**, 1591-1594, doi:10.1126/science.1236425 (2013).

470 35 Lubke, J. & Feldmeyer, D. Excitatory signal flow and connectivity in a cortical column: focus on barrel
471 cortex. *Brain Struct Funct* **212**, 3-17, doi:10.1007/s00429-007-0144-2 (2007).

472 36 Hay, Y. A., Lambolez, B. & Tricoire, L. Nicotinic Transmission onto Layer 6 Cortical Neurons Relies
473 on Synaptic Activation of Non-alpha7 Receptors. *Cereb Cortex* **26**, 2549-2562,
474 doi:10.1093/cercor/bhv085 (2016).

475 37 Kassam, S. M., Herman, P. M., Goodfellow, N. M., Alves, N. C. & Lambe, E. K. Developmental
476 excitation of corticothalamic neurons by nicotinic acetylcholine receptors. *J Neurosci* **28**, 8756-8764,
477 doi:10.1523/JNEUROSCI.2645-08.2008 (2008).

478 38 Alves, N. C., Bailey, C. D., Nashmi, R. & Lambe, E. K. Developmental sex differences in nicotinic
479 currents of prefrontal layer VI neurons in mice and rats. *PLoS One* **5**, e9261,
480 doi:10.1371/journal.pone.0009261 (2010).

481 39 Bailey, C. D., Alves, N. C., Nashmi, R., De Biasi, M. & Lambe, E. K. Nicotinic alpha5 subunits drive
482 developmental changes in the activation and morphology of prefrontal cortex layer VI neurons. *Biol*
483 *Psychiatry* **71**, 120-128, doi:10.1016/j.biopsych.2011.09.011 (2012).

484 40Tian, M. K., Bailey, C. D. & Lambe, E. K. Cholinergic excitation in mouse primary vs. associative cortex:
485 region-specific magnitude and receptor balance. *Eur J Neurosci* **40**, 2608-2618, doi:10.1111/ejn.12622
486 (2014).

487 41 Gulledge, A. T. & Stuart, G. J. Cholinergic inhibition of neocortical pyramidal neurons. *J Neurosci* **25**,
488 10308-10320, doi:10.1523/JNEUROSCI.2697-05.2005 (2005).

489 42 Gulledge, A. T. & Kawaguchi, Y. Phasic cholinergic signaling in the hippocampus: functional homology
490 with the neocortex? *Hippocampus* **17**, 327-332, doi:10.1002/hipo.20279 (2007).

491 43 Dasari, S., Hill, C. & Gulledge, A. T. A unifying hypothesis for M1 muscarinic receptor signalling in
492 pyramidal neurons. *J. Physiol.* **595**, 1711-1723, doi:10.1113/JP273627 (2017).

493 44 Mercer, A. *et al.* Excitatory connections made by presynaptic cortico-cortical pyramidal cells in layer 6
494 of the neocortex. *Cereb Cortex* **15**, 1485-1496, doi:10.1093/cercor/bhi027 (2005).

495 45 Narayanan, R. T. *et al.* Beyond Columnar Organization: Cell Type- and Target Layer-Specific Principles
496 of Horizontal Axon Projection Patterns in Rat Vibrissal Cortex. *Cereb. Cortex* **25**, 4450-4468,
497 doi:10.1093/cercor/bhv053 (2015).

498 46 Tasic, B. *et al.* Adult mouse cortical cell taxonomy revealed by single cell transcriptomics. *Nat Neurosci*
499 **19**, 335-346, doi:10.1038/nn.4216 (2016).

500 47 Gil, Z., Connors, B. W. & Amitai, Y. Differential regulation of neocortical synapses by neuromodulators
501 and activity. *Neuron* **19**, 679-686 (1997).

502 48 Levy, R. B., Reyes, A. D. & Aoki, C. Nicotinic and muscarinic reduction of unitary excitatory
503 postsynaptic potentials in sensory cortex; dual intracellular recording in vitro. *J Neurophysiol* **95**, 2155-
504 2166, doi:10.1152/jn.00603.2005 (2006).

505 49 West, D. C., Mercer, A., Kirchhecker, S., Morris, O. T. & Thomson, A. M. Layer 6 cortico-thalamic
506 pyramidal cells preferentially innervate interneurons and generate facilitating EPSPs. *Cereb Cortex* **16**,
507 200-211, doi:10.1093/cercor/bhi098 (2006).

508 50 Crandall, S. R., Patrick, S. L., Cruikshank, S. J. & Connors, B. W. Infrabarrels Are Layer 6 Circuit
509 Modules in the Barrel Cortex that Link Long-Range Inputs and Outputs. *Cell Rep* **21**, 3065-3078,
510 doi:10.1016/j.celrep.2017.11.049 (2017).

511 51 Parikh, V., Kozak, R., Martinez, V. & Sarter, M. Prefrontal acetylcholine release controls cue detection
512 on multiple timescales. *Neuron* **56**, 141-154, doi:10.1016/j.neuron.2007.08.025 (2007).

513 52 Sarter, M., Parikh, V. & Howe, W. M. Phasic acetylcholine release and the volume transmission
514 hypothesis: time to move on. *Nat Rev Neurosci* **10**, 383-390, doi:10.1038/nrn2635 (2009).

515 53 Colquhoun, D. & Sakmann, B. Fast events in single-channel currents activated by acetylcholine and its
516 analogues at the frog muscle end-plate. *J Physiol* **369**, 501-557, doi:10.1113/jphysiol.1985.sp015912
517 (1985).

518 54 Mazzaferro, S., Bermudez, I. & Sine, S. M. alpha4beta2 Nicotinic acetylcholine receptors: Relationships
519 between subunit stoichiometry and function at the single chanel level. *J Biol Chem* **292**, 2729-2740,
520 doi:10.1074/jbc.M116.764183 (2017).

521 55 Fucile, S. Ca2+ permeability of nicotinic acetylcholine receptors. *Cell Calcium* **35**, 1-8 (2004).

522 56 Hasselmo, M. E. & McGaughy, J. High acetylcholine levels set circuit dynamics for attention and
523 encoding and low acetylcholine levels set dynamics for consolidation. *Prog Brain Res* **145**, 207-231,
524 doi:10.1016/S0079-6123(03)45015-2 (2004).

525 57 Bennett, C., Arroyo, S., Berns, D. & Hestrin, S. Mechanisms generating dual-component nicotinic
526 EPSCs in cortical interneurons. *J Neurosci* **32**, 17287-17296, doi:10.1523/JNEUROSCI.3565-12.2012
527 (2012).

528 58 Takacs, V. T., Freund, T. F. & Nyiri, G. Neuroligin 2 is expressed in synapses established by cholinergic
529 cells in the mouse brain. *PLoS One* **8**, e72450, doi:10.1371/journal.pone.0072450 (2013).

530 59 Gulledge, A. T., Park, S. B., Kawaguchi, Y. & Stuart, G. J. Heterogeneity of phasic cholinergic signaling
531 in neocortical neurons. *J Neurophysiol* **97**, 2215-2229, doi:10.1152/jn.00493.2006 (2007).

532 60 Dembrow, N. C., Chitwood, R. A. & Johnston, D. Projection-specific neuromodulation of medial
533 prefrontal cortex neurons. *The Journal of neuroscience : the official journal of the Society for*
534 *Neuroscience* **30**, 16922-16937, doi:10.1523/JNEUROSCI.3644-10.2010 (2010).

535 61 van Aerde, K. I., Qi, G. & Feldmeyer, D. Cell Type-Specific Effects of Adenosine on Cortical Neurons.
536 *Cerebral cortex*, doi:10.1093/cercor/bht274 (2013).

537 62 Clarkson, R. L., Liptak, A. T., Gee, S. M., Sohal, V. S. & Bender, K. J. D3 Receptors Regulate
538 Excitability in a Unique Class of Prefrontal Pyramidal Cells. *J Neurosci* **37**, 5846-5860,
539 doi:10.1523/JNEUROSCI.0310-17.2017 (2017).

540 63 Anastasiades, P. G., Boada, C. & Carter, A. G. Cell-Type-Specific D1 Dopamine Receptor Modulation
541 of Projection Neurons and Interneurons in the Prefrontal Cortex. *Cereb Cortex*,
542 doi:10.1093/cercor/bhy299 (2018).

543 64 Baker, A. L., O'Toole, R. J. & Gulledge, A. T. Preferential cholinergic excitation of corticopontine
544 neurons. *J Physiol* **596**, 1659-1679, doi:10.1113/JP275194 (2018).

545 65 Lambe, E. K., Picciotto, M. R. & Aghajanian, G. K. Nicotine induces glutamate release from
546 thalamocortical terminals in prefrontal cortex. *Neuropsychopharmacology* **28**, 216-225,
547 doi:10.1038/sj.npp.1300032 (2003).

548 66 Kawai, H., Lazar, R. & Metherate, R. Nicotinic control of axon excitability regulates thalamocortical
549 transmission. *Nat Neurosci* **10**, 1168-1175, doi:10.1038/nn1956 (2007).

550 67 Hsieh, C. Y., Cruikshank, S. J. & Metherate, R. Differential modulation of auditory thalamocortical and
551 intracortical synaptic transmission by cholinergic agonist. *Brain Res* **880**, 51-64 (2000).

552 68 Oldford, E. & Castro-Alamancos, M. A. Input-specific effects of acetylcholine on sensory and
553 intracortical evoked responses in the "barrel cortex" in vivo. *Neuroscience* **117**, 769-778 (2003).

554 69 Gray, R., Rajan, A. S., Radcliffe, K. A., Yakehiro, M. & Dani, J. A. Hippocampal synaptic transmission
555 enhanced by low concentrations of nicotine. *Nature* **383**, 713-716, doi:10.1038/383713a0 (1996).

556 70 Mansvelder, H. D. & McGehee, D. S. Long-term potentiation of excitatory inputs to brain reward areas
557 by nicotine. *Neuron* **27**, 349-357 (2000).

558 71 Urban-Ciecko, J., Jouhanneau, J. S., Myal, S. E., Poulet, J. F. A. & Barth, A. L. Precisely Timed Nicotinic
559 Activation Drives SST Inhibition in Neocortical Circuits. *Neuron* **97**, 611-625 e615,
560 doi:10.1016/j.neuron.2018.01.037 (2018).

561 72 Agmon, A. & Connors, B. W. Thalamocortical responses of mouse somatosensory (barrel) cortex in
562 vitro. *Neuroscience* **41**, 365-379 (1991).

563 73 Marx, M., Gunter, R. H., Hucko, W., Radnikow, G. & Feldmeyer, D. Improved biocytin labeling and
564 neuronal 3D reconstruction. *Nat Protoc* **7**, 394-407, doi:10.1038/nprot.2011.449 (2012).

565 74 Qi, G. X., Radnikow, G. & Feldmeyer, D. Electrophysiological and Morphological Characterization of
566 Neuronal Microcircuits in Acute Brain Slices Using Paired Patch-Clamp Recordings. *Jove-J Vis Exp*,
567 doi:ARTN e52358 10.3791/52358 (2015).

568 75 Dodt, H. U. & Zieglgansberger, W. Visualizing unstained neurons in living brain slices by infrared DIC-
569 videomicroscopy. *Brain Res* **537**, 333-336 (1990).

570 76 Meyer, H. S. *et al.* Number and laminar distribution of neurons in a thalamocortical projection column
571 of rat vibrissal cortex. *Cereb Cortex* **20**, 2277-2286, doi:10.1093/cercor/bhq067 (2010).

572 77 Feldmeyer, D., Egger, V., Lubke, J. & Sakmann, B. Reliable synaptic connections between pairs of
573 excitatory layer 4 neurones within a single 'barrel' of developing rat somatosensory cortex. *J Physiol* **521**
574 **Pt 1**, 169-190 (1999).

575
576

577

578 ## Materials and Methods

579 ### Slice preparation and solutions for electrophysiology

580 All experiments involving animals were performed in accordance with the EU Directive
581 2010/63/EU, the German animal welfare act and the guidelines of the Federation of European
582 Laboratory Animal Science Association (FELASA). Wistar rats (Charles River) were maintained
583 on a 12/12-hr light-dark cycle from 7 AM to 7 PM. Rats aged 17-21 postnatal days (P17-21, both
584 sexes) were lightly anaesthetized with a concentration < 0.1% of isoflurane and then decapitated.
585 The brain was quickly removed and transferred into ice-cold artificial cerebrospinal fluid (ACSF)
586 containing a high Mg^{2+}- and a low Ca^{2+}-concentration (4 mM $MgCl_2$ and 1 mM $CaCl_2$) to reduce
587 synaptic activity and bubbled continuously with carbogen (95% O_2 and 5% CO_2). It was then placed
588 on the ramp of a slope of 10° and were cut at an angle of 50° to the midline[72]. Thalamocortical
589 slices were cut at 350 µm thickness using a high vibration frequency and incubated for 30-60
590 minutes at room temperature (21-24°C) in slicing solution. During whole-cell patch clamp
591 recordings, slices were continuously perfused with a perfusion solution containing (in mM): 125
592 NaCl, 2.5 KCl, 25 D-glucose, 25 $NaHCO_3$, 1.25 NaH_2PO_4, 2 $CaCl_2$, 1 $MgCl_2$, 3 myo-inositol, 2
593 sodium pyruvate and 0.4 ascorbic acid, bubbled with carbogen and maintained at a temperature of
594 30-33°C. Patch pipettes were filled with an internal solution containing (in mM): 135 K gluconate,
595 4 KCl, 10 HEPES, 10 phosphocreatine, 4 Mg-ATP and 0.3 GTP (pH 7.4, 290-300 mOsm). To stain
596 the patched neurons, biocytin was added at a concentration between 3-5 mg/ml to the pipette
597 solution; a recording time of ~15-30 minutes was necessary for biocytin to diffuse into the dendrites
598 and axons of the recorded cells[73,74]. No biocytin was added to the internal solution of 'searching'
599 pipettes used during searching for synaptic connections.

600

601 ### Cell identification

602 Slices were placed in the recording chamber under an upright microscope (fitted with 4x plan/ 0.13
603 numerical aperture and 40x water immersion/0.80 NA objectives; Olympus, Tokyo, Japan) with
604 the pial surface pointing forward. The cortical layers and the barrel field were visualized at 4x
605 magnification; the barrels can be identified in L4 as narrow dark stripes with evenly spaced, light
606 'hollows' and were visible in 6-8 consecutive slices. L6A neurons were identified in the upper 60%
607 of layer 6 at 40x magnification using infrared differential interference contrast (IR-DIC)
608 microscope[75,76]. Putative PCs and interneurons were differentiated on the basis of their intrinsic

609 action potential firing pattern during recording and after histological processing by their
610 morphological appearance.
611
612 **Electrophysiological recordings**
613 Whole-cell patch clamp recordings from L6A neurons were performed at 30-33°C for an optimal
614 oxygenation. Patch pipettes were pulled from thick-wall borosilicate capillaries (outer diameter: 2
615 mm; inner diameter: 1 mm) to a final resistance of 6-10 MΩ. Recordings were made using an
616 EPC10 amplifier (HEKA, Lambrecht, Germany), sampled at 10 kHz, and filtered at 2.9 kHz using
617 the Patch-master software (HEKA). Neurons were selected randomly and excluded from the
618 analysis when their whole-cell series resistance exceeded 40 MΩ (50 MΩ for neurons from paired-
619 recodings) or their resting membrane potential was more depolarized than -50 mV immediately
620 after rupturing the cell membrane. The resting membrane potential of L6A excitatory neurons was
621 continuously recorded in the current clamp mode to monitor changes in amplitude.
622 Miniature spontaneous events were recorded in voltage-clamp mode and changes in mEPSC
623 frequency and amplitude were analyzed. Recordings of L6A excitatory neurons were made in the
624 presence of tetrodotoxin (TTX, 0.5 µM) and gabazine (10 µM) to inhibit AP firing and inhibitory
625 postsynaptic currents (IPSCs), respectively. During recordings, the holding potential was set at -
626 70mV.
627 Because the connectivity of L6A neurons was low compared to other intra-laminar connections in
628 rat barrel cortex, we followed the 'searching procedure' described previously after patching a
629 putative postsynaptic neuron[74,77]. A monosynaptic connection can be found by patching multiple
630 cells in 'loose cell-attached' mode. When the AP resulted in a unitary excitatory postsynaptic
631 potential (uEPSP) in the postsynaptic L6A neuron, this presynaptic neuron was repatched with a
632 new pipette filled with biocytin containing internal solution. APs were elicited by current injection
633 in the presynaptic neurons and the postsynaptic response were recorded in whole cell (current
634 clamp) mode, the effects of ACh on unitary EPSPs were then tested.
635
636 **Drug Application**
637 ACh (1 µM-10 mM) was bath applied via the perfusion system or puff applied through a patch
638 pipette (tip diameter: 1-2 µm) connected to a PDES-02D device (npi electronic GmbH, Tamm,

639 Germany). The puff pipette was placed at 10-20 µm from the same recorded neuron and a brief
640 low pressure was applied for about 1 s. Mecamylamine (10 µM), atropine (200 nM-20 µM),
641 pirenzepine (0.5 µM), tropicamide (1µM), dihydro-ß-erythroidine (DHßE) (10 µM),
642 methyllycaconitine (MLA) (10µM), tetrodotoxin (TTX) (0.5 µM) and gabazine (10 µM) were all
643 bath applied; drugs were purchased from Sigma-Aldrich (Steinheim, Germany) or Tocris (Bristol,
644 UK).

645

646 **Histological staining**

647 After single cell or paired recordings, brain slices containing biocytin-filled neurons were
648 processed as described previously[73]. Slices were fixed at 4°C for at least 12 hours in 100 mM
649 phosphate buffer (PB, PH 7.4) solution containing 4% paraformaldehyde (PFA) and then incubated
650 in 0.1% triton X-100 solution containing avidin-biotinylated horseradish peroxidase (Vector ABC
651 staining kit, Vector Lab. Inc., Burlingame, USA). The reaction was catalyzed using 3,3′-
652 diaminobenzidine (Sigma-Aldrich, St. Louis, MO, USA) as a chromogen. Slices were again rinsed
653 with 100 mM PB solution several times, followed by slow dehydration using ethanol and xylene.
654 After embedding in Eukitt medium (Otto Kindler GmbH, Freiburg, Germany), the dendritic and
655 axonal structures were clearly visible.

656 Immunofluorescence staining was performed for the identification of molecular markers expressed
657 in L6A PCs. During electrophysiological recordings, Alexa Fluor® 594 dye (1:500, Invitrogen,
658 Darmstadt, Germany) was added to the internal solution for post hoc identification of patched
659 neurons. After recording, slices (350 µm) were fixed with 4% PFA in 100mM PBS for at least 24
660 hours at 4°C and then permeabilized in 1% milk power solution containing 0.5% Triton X-100 and
661 100 mM PBS. Primary and secondary antibodies were diluted in the permeabilization solution (0.5%
662 Triton X-100 and 100 mM PBS) shortly before experiments. For single cell-FoxP2 staining, slices
663 were incubated overnight with Goat-anti-FoxP2 primary antibody (1:500, Santa Cruz
664 Biotechnology, Heidelberg, Germany) at 4°C and then rinsed thoroughly with 100 mM PBS.
665 Subsequently, slices were treated with Alexa Fluor® secondary antibodies (1:500) for 2-3 hours at
666 room temperature in the dark. After being rinsed in 100 mM PBS the slices were embedded in
667 Moviol. The fluorescence images were taken using the Olympus CellSens platform. The position
668 of the patched neurons were identified by the conjugated Alexa dye, so that the expression of FoxP2
669 could be tested in biocytin-stained neurons. After acquiring fluorescent images, slices were

670 incubated in 100 mM PBS overnight and were processed for subsequent morphological analysis.
671 Co-immunostaining of FoxP2 and M_4Rs (Rabbit-anti-M_4Rs, 1:500, Abbexa, Cambridge, UK) were
672 performed with 150 µm thin brain slices following the procedure described above.
673

674 **Morphological reconstructions**

675 3D reconstructions of L6A excitatory and inhibitory neurons or synaptically coupled neuron pairs
676 labelled with biocytin were made using the NEUROLUCIDA® software (MicroBrightField Inc.,
677 Williston, VT, USA) and Olympus BX61 microscopy at 1000 X magnification. Slices were
678 selected to be reconstructed only if the labeling quality was high and the background staining was
679 low. Barrel borders, demarcation of different layers, pial surface and white matter were delineated
680 during reconstructions. The cell body, the axonal and dendritic branches were reconstructed
681 manually under constant visual inspection to detect even small collaterals. Corrections for
682 shrinkage were performed in all spatial dimensions (factor 1.1 in the x and y axes, factor 2.1 in the
683 z axes) 73. Analysis of 3D reconstructed neurons was done with NEUROEXPLORER® software
684 (MicroBrightField Inc., Williston, VT, USA).
685

686 The neuronal polarity of reconstruction was calculated with NEUROEXPLORER® software using
687 cubic spline smoothing. The dendritic and axonal length was averaged for each of the 120 "3°
688 sectors" around the soma. Data were recalculated, plotted in angular subdivision around the soma
689 and polar plots were made with Grapher software (GoldenSoftware, Colorado, USA). The radian
690 depicts degree in angles (°) with 0° towards the pial surface, 90° towards the posterior-median axis,
691 180° towards the white matter, and 270° towards the anterior-lateral axis.
692

693 **Data analysis**

694 Custom written macros for Igor Pro 6 (WaveMetrics, Lake Oswego, USA) were used to analyze
695 the recorded electrophysiological signals. The miniature spontaneous activity was analyzed using
696 the program SPCN (http://www.spacan.net). A threshold of 5 pA was set manually for detecting
697 mEPSC events, which is at least 2.5 fold larger than the noise level (< 2pA). No noise filtration
698 was applied before data analysis.

699 The synaptic properties were evaluated as described in the previous studies[77]. First, all sweeps were
700 aligned to their corresponding presynaptic AP peaks and an average sweep was generated as the

701 mean uEPSP. The EPSP amplitude was calculated as the difference between the mean baseline
702 amplitude and maximum voltage of the postsynaptic event. The paired pulse ratio was defined as
703 the second uPSP amplitude divided by the first uPSP amplitude of the mean uPSP elicited by paired
704 APs with a stimulation frequency of 10 Hz. Failures were defined as events with amplitudes <1.5×
705 the standard deviation (SD) of the noise within the baseline window and the failure rate refers to
706 the percentage of failures. The coefficient of variation (CV) was calculated as the SD divided by
707 the mean uEPSP amplitude.

708

709 **Statistical tests**

710 For all data, the mean ± SD was given. To assess the differences between two paired groups under
711 different pharmacological conditions, Wilcoxon signed rank test was performed. The paired
712 Student's *t* test was used when n = 4 for the paired samples and the Mann-Whitney *U*-test was used
713 when the sample size was different between two groups. Statistical significance was set at $P < 0.05$,
714 n indicates the number of neurons or pairs analyzed.

Figures

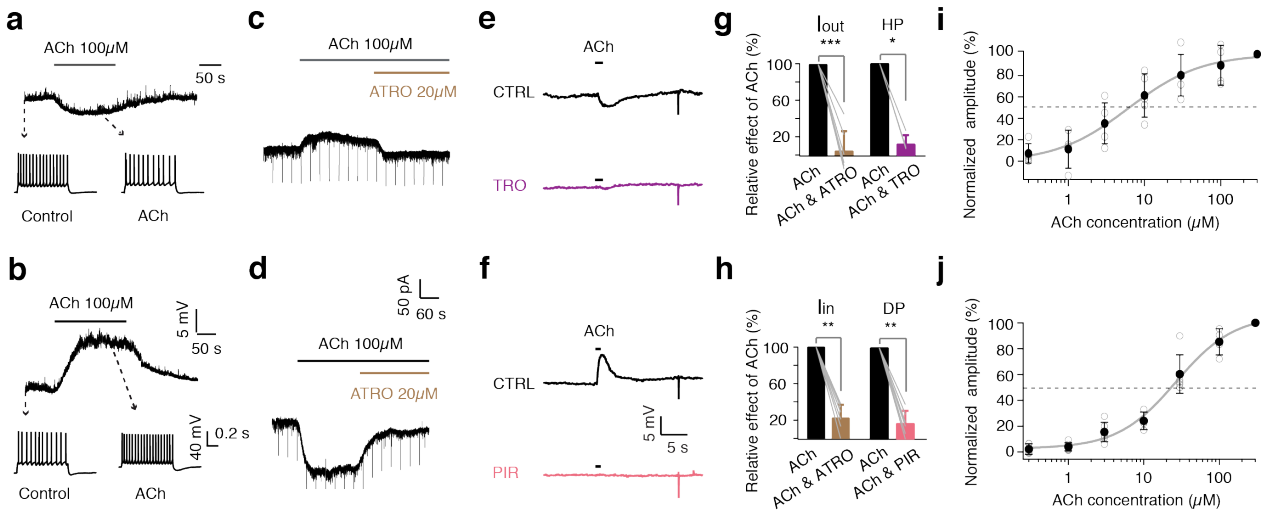

Fig. 1 Low concentrations of ACh induce either a hyperpolarization or a depolarization of L6A PCs by activating mAChRs.

(a, b) Top, L6A PC either show a hyperpolarizing (a) or a depolarizing (b) response following bath application of 100 μM ACh. Bottom, firing patterns of neurons in response to 1 s depolarising current injection (rheobase + 100 pA) before and during ACh application.

(c, d) Representative voltage-clamp recordings with bath application of ACh showing outward current (I_{out}) (e) or inward current (I_{in}) (f) in L6A PCs. The effects are blocked by 20 μM atropine (ATRO).

(e, f) Representative current-clamp recordings showing that puff application of ACh (100μM) evokes a fast hyperpolarization (HP) (g) or depolarization (DP) (h) in L6A PCs. The specific M_1 mAChR antagonist pirenzipine (PIR, 0.5 μM) or the specific M_4 mAChR antagonist tropicamide (TRO, 1 μM), respectively, were added to the perfusion solution to block ACh-induced membrane potential changes.

(g, h) Summary bar graphs showing the percentage block by general and specific mAChR antagonists. n = 7, p = 0.0006 for I_{out} group, n = 7, p = 0.0022 for I_{in} group, n = 4, p = 0.029 for HP group and n = 6, p = 0.0022 for DP group. Statistical analysis was performed using Mann Whitney *U*-test . Error bars represent SD.

(i, j) Muscarinic responses of ACh were examined in the presence of 1 μM mecamylamine (MEC) and 0.5 μM TTX. ACh dose-response curves for hyperpolarizing (n = 5) (c) and depolarizing (n = 8) (d) L6A PCs are fitted by the Hill equation. Dashed lines represent half maximal effects. The corresponding EC_{50} is 6.2 ± 1.3 μM for hyperpolarizing PCs and 26.7 ± 5.4 μM for depolarizing PCs. Filled circles represent mean values of different ACh concentrations.

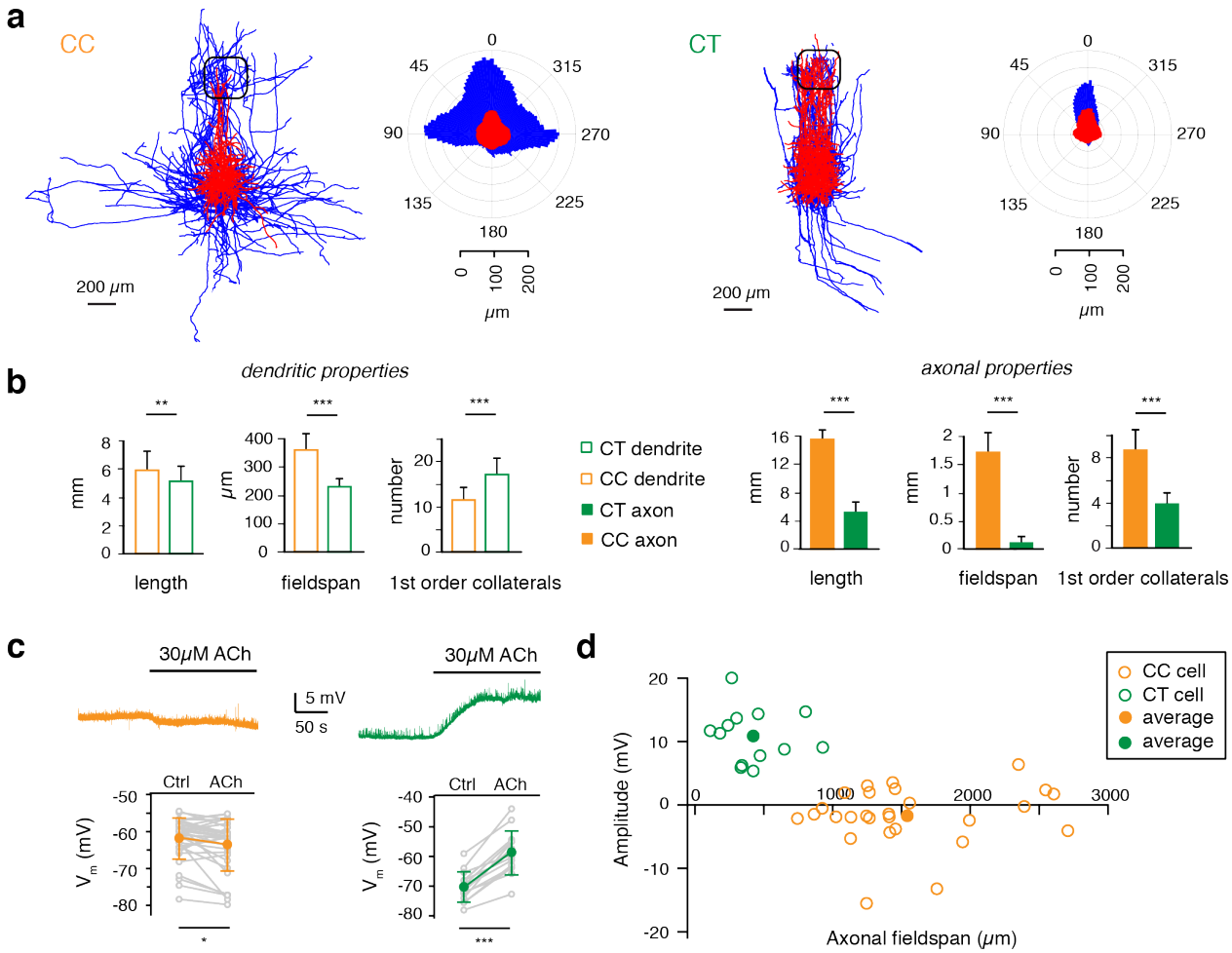

Fig. 2 ACh hyperpolarizes CC L6A PCs but depolarizes CT L6A PCs.

(a) Left, overlay of reconstructions of CC and CT PCs. Reconstructions of PCs were aligned with respect to the barrel center. Right, polar plots of CC and CT PCs. n = 15 for each group. Somatodendrites are shown in red and axons are shown in blue.

(b) Histograms comparing the length, fieldspan and number of first order collaterals of axonal and dendritic structures for the two groups of PCs. n = 21 for CC neurons and n = 54 for CT neurons. Dendritic length: $p = 0.0015$, dendritic fieldspan: $p = 1.4 \times 10^{-10}$, number of dendritic main nodes: $p = 1.7 \times 10^{-6}$; Axonal length: $p = 9.6 \times 10^{-8}$, dendritic fieldspan: $p = 4.8 \times 10^{-11}$, number of axoanl main nodes: $p = 8.5 \times 10^{-11}$ for Mann-Whitney *U*-test.

(c) Top, representative current-clamp recordings of a depolarizing CC (orange) and a hyperpolarizing CT pyramidal cell (green) following bath application of 30μM ACh. Bottom, histograms of resting membrane potential (V_m) of L6A CC PCs in control and in the presence of 30 μM ACh (n = 35, $p = 0.019$ for Wilcoxon signed-rank test) and CT (n = 14, $p = 6.1 \times 10^{-5}$ for Wilcoxon signed-rank test) PCs.

(d) Plots of the ACh-induced change in V_m vs axonal fieldspan for two subtypes of PCs. Open orange circles, data from individual CC PCs (n = 27); open green circles, data from individual CT PCs (n = 13). Filled orange circle, average data from CC cells; filled green circle, average data from CT cells.

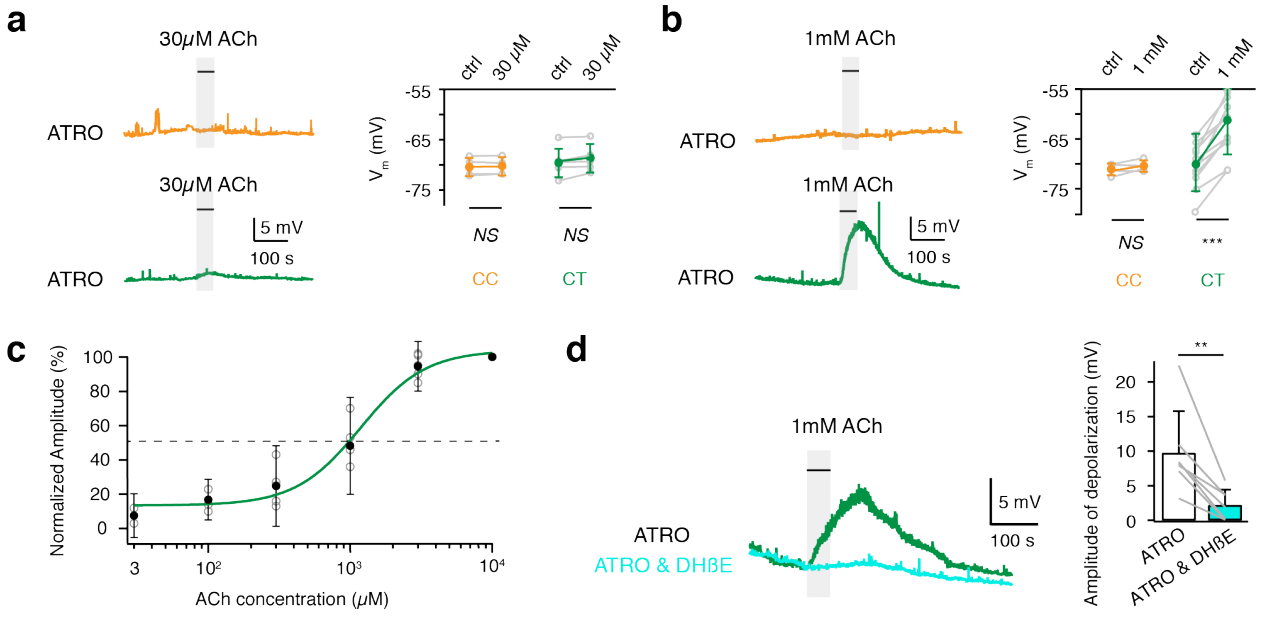

Fig. 3 High concentration of ACh selectively depolarizes CT PCs.

(a) In the presence of 200 nM atropine (ATRO), bath application of low concentration ACh (30 μM, 50s) show no effect on either CC (top) or CT (bottom) PCs. Summary plots show the resting membrane potential (V_m) under control and ACh conditions in L6A CC (n = 5, p = 0.188) and CT (n = 5, p = 0.0625) PCs. NS (not significant) for Wilcoxon signed-rank test. Error bars represent SD.

(b) In the presence of 200 nM ATRO, bath application of 1 mM ACh for 50s has no effect on CC L6A PCs (top) but induces a strong depolarization of CT L6A PCs (bottom). Summary plots showing V_m of CC L6A PCs under control conditions and in the presence of ACh in L6A CC (n = 5, p = 0.156) and CT (n = 12, p = 0.0002) PCs. Statistical analysis was peformed using Wilcoxon signed-rank test. Error bars represent SD.

(c) The dose-response curve of ACh under ATRO application (200 nM) in CT PCs (n = 5) is well fitted by the Hill equation. The dashed line indicates the half maximal effect; the corresponding EC_{50} is 1.2 mM. Filled circles show mean effect of different concentrations while open circles represent individual values. Error bars represent SD.

(d) The depolarization induced by ACh application (in the presence of 200 nM ATRO) is blocked by 10 μM of the specific antagonist of $\alpha_4\beta_2$ subunit-containing nAChRs DHβE in CT L6A PCs. Summary plots showing the amplitude of the depolarization in response to application of 1 mM ACh in the presence of ATRO alone (open bar) and ATRO together with DHβE (n = 7, p = 0.0078 for Wilcoxon signed-rank test). Error bars represent SD.

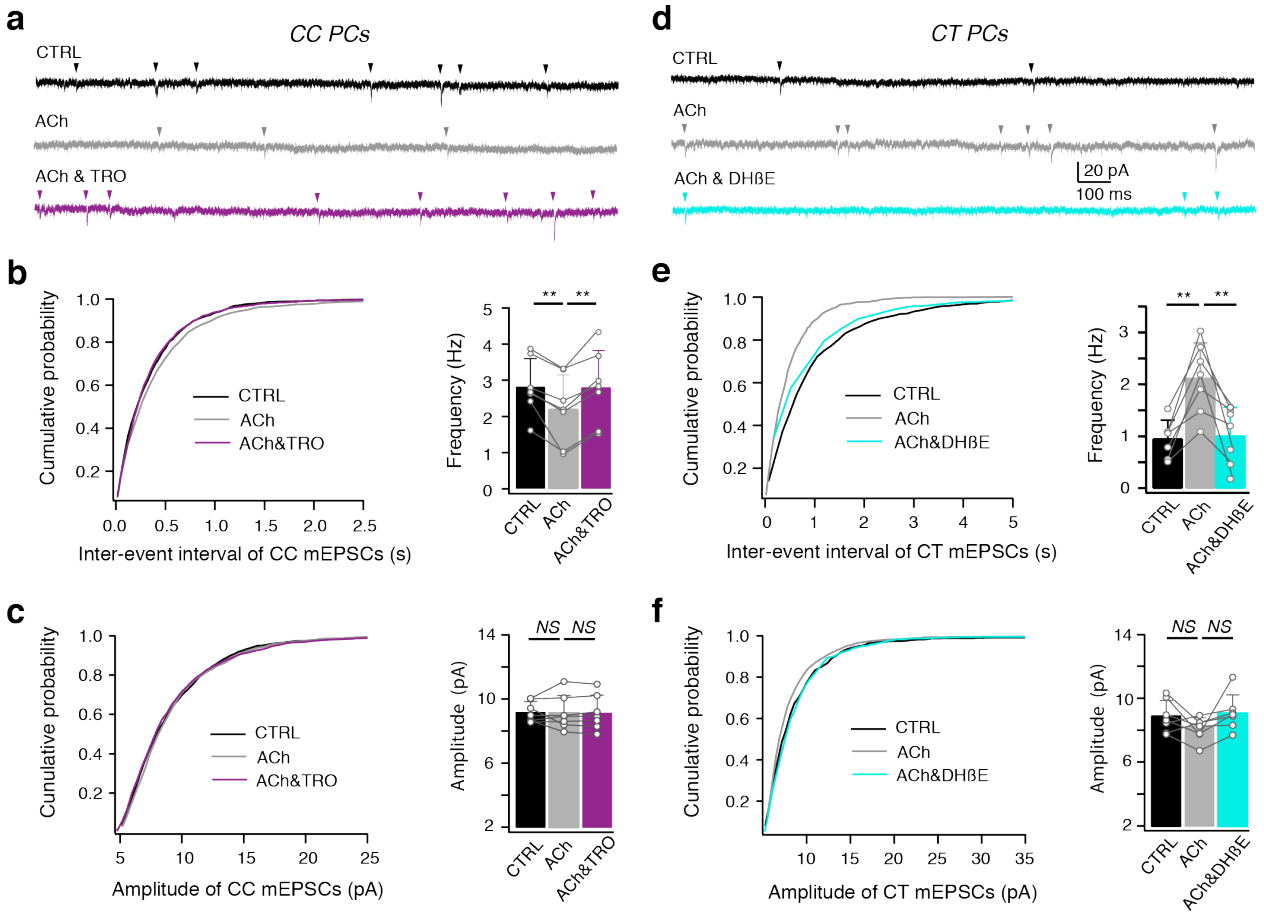

Fig. 4 ACh differentially modulates miniature spontaneous activity in CC and CT L6A PCs.

(a) Example voltage-clamp recordings of a CC L6A PCs under control (black), bath application of 30 µM ACh (gray) and co-application of ACh and 1 µM TRO (purple). Miniature EPSCs were recorded in the presence of TTX (0.5 µM) and GABAzine (10 µM) at a holding potential of -70 mV.

(b) Cumulative distributions of mEPSCs inter-event interval recorded in CC L6A PCs under control condition, in the presence of ACh alone, and of ACh & TRO. Summary histograms of mEPSC frequency are shown on the right. **P < 0.01 for Wilcoxon signed-rank test. Error bars represent SD.

(c) Cumulative distributions of mEPSCs amplitude recorded in CC L6A PCs under control, ACh and ACh & TRO conditions. Summary histograms of mEPSC amplitude are shown on the right. Control vs. ACh, p = 0.8125; ACh vs. ACh & TRO, p = 0.9375, n = 7 for Wilcoxon signed-rank test. Error bars represent SD.

(d) Example voltage-clamp recordings of a CT L6A PC in control (black), after bath application of 30 µM ACh (gray) and subsequent co-application of ACh and 10 µM DHßE (turquoise). Miniature EPSCs were recorded in the presence of TTX (0.5 µM) and GABAzine (10 µM) at a holding potential of -70 mV.

(e) Cumulative distributions of mEPSCs inter-event interval recorded in CT L6A PCs under control, ACh and ACh & DHßE conditions. Summary histograms of mEPSC frequency are shown on the right. **$P < 0.01$ for Wilcoxon signed-rank test. Error bars represent SD.

(f) Cumulative distributions of mEPSCs amplitude recorded in CT L6A PCs under control, ACh and ACh & DHßE conditions. Summary histograms of mEPSC amplitude are shown on the right. Control vs. ACh, $p = 0.4258$; ACh vs. ACh & DHßE, $p = 0.0781$, $n = 7$ for Wilcoxon signed-rank test. Error bars represent SD.

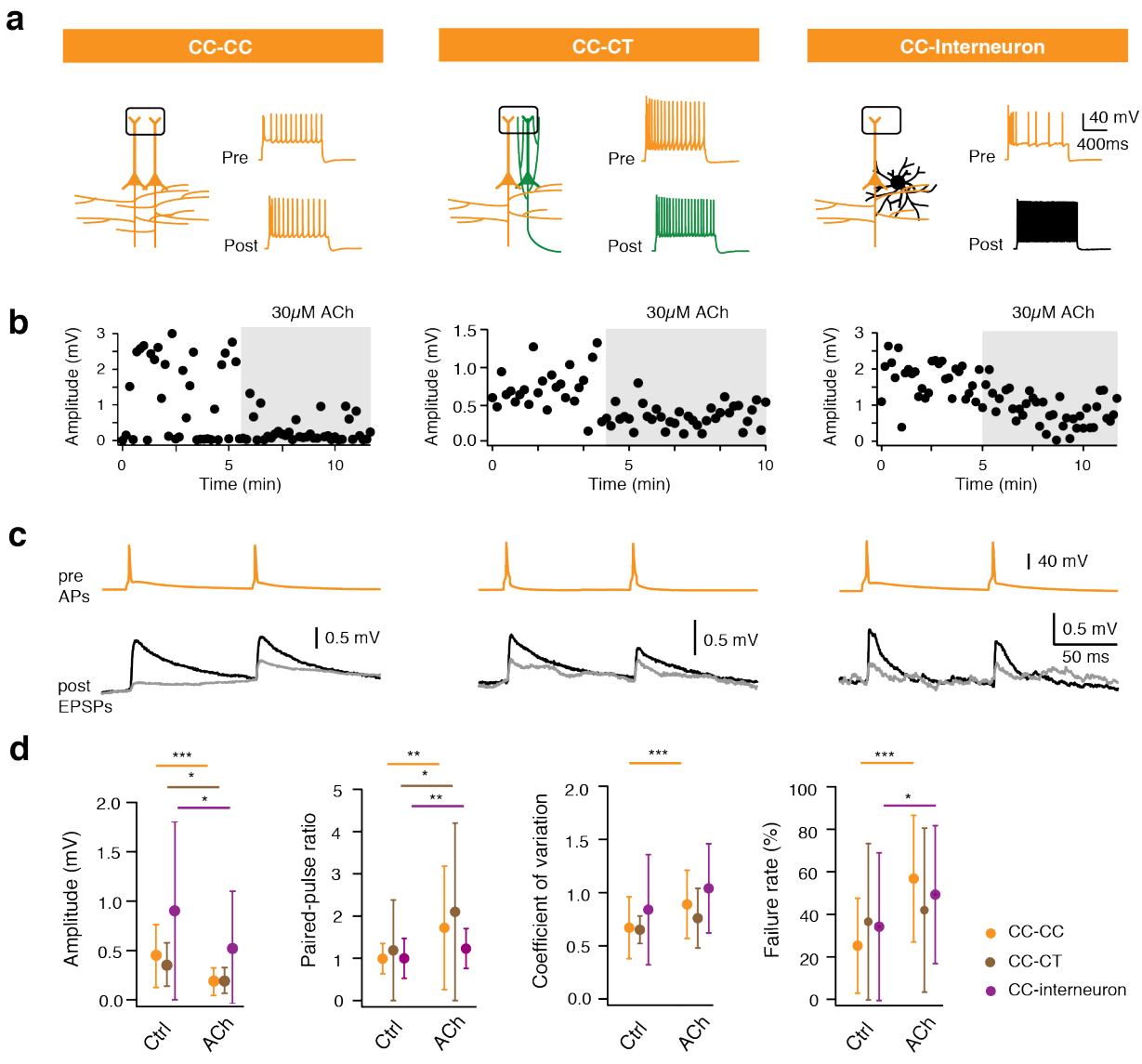

Fig. 5 ACh-mediated reduction of presynaptic release at CC PC synapses.

(a) Left, Schematic representation of the synaptic connections with a presynaptic CC L6A PC. CC PCs are shown in orange, the CT PC in green and the interneuron in black. Barrel structures indicate layer 4. Right, corresponding firing patterns of pre- and postsynaptic neurons of the same connection type.

(b) Time course of EPSP amplitude changes following bath application of 30μM ACh (gray phases) in a CC-CC, a CC-CT and a CC-interneuron pair.

(c) Overlay of average EPSPs in control (black) and ACh application (gray) phases. Presynaptic APs are shown at the top. Data are recorded from the same pairs as in (b).

(d) The average and SD of several EPSP properties for CC-CC (n = 20), CC-CT (n = 5) and CC-interneuron (n = 9) connections are shown. *P < 0.05, **P < 0.01, ***P < 0.001 for Wilcoxon signed-rank test.

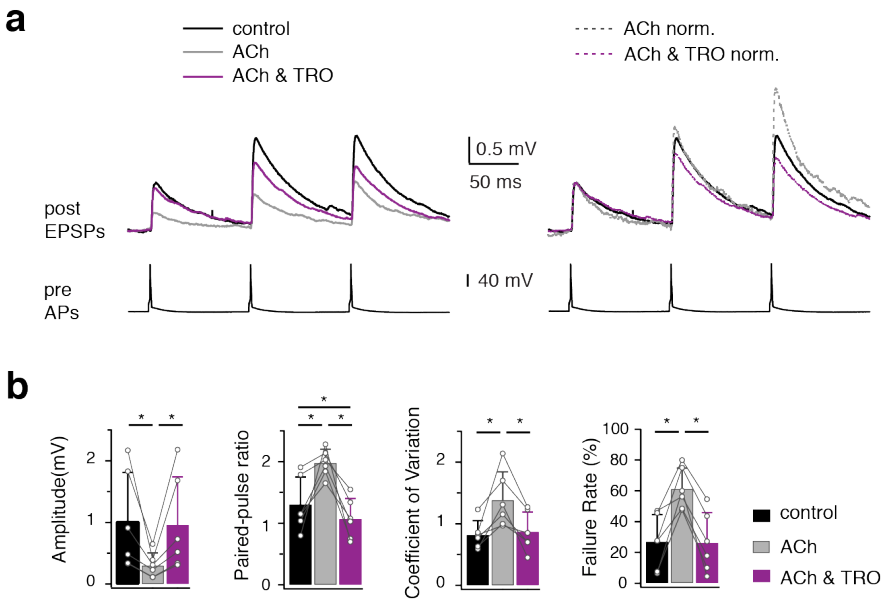

Fig. 6 ACh decreases presynaptic release probability of CC PC via activation of M_4 AChRs.

(a) Left, Overlay of average EPSPs recorded in control, the presence of ACh (30µM), and of ACh & TRO (1 µM) from a representative CC-CC connection. Right, normalising the mean EPSP amplitudes obtained in ACh and ACh & TRO to the first EPSPs amplitude in control reveals changes of PPR. Presynaptic APs are shown at the bottom.

(b) Histograms (n = 6) showing the effect of ACh and TRO blockade of ACh-induced changes on several EPSP properties including EPSP amplitude, PPR, CV and failure rate. Data were recorded from L6A synaptic connections with a presynaptic CC PC. Open circles, individual data points; bars, the average for each condition. Error bars represent SD. *P < 0.05 for Wilcoxon signed-rank test.

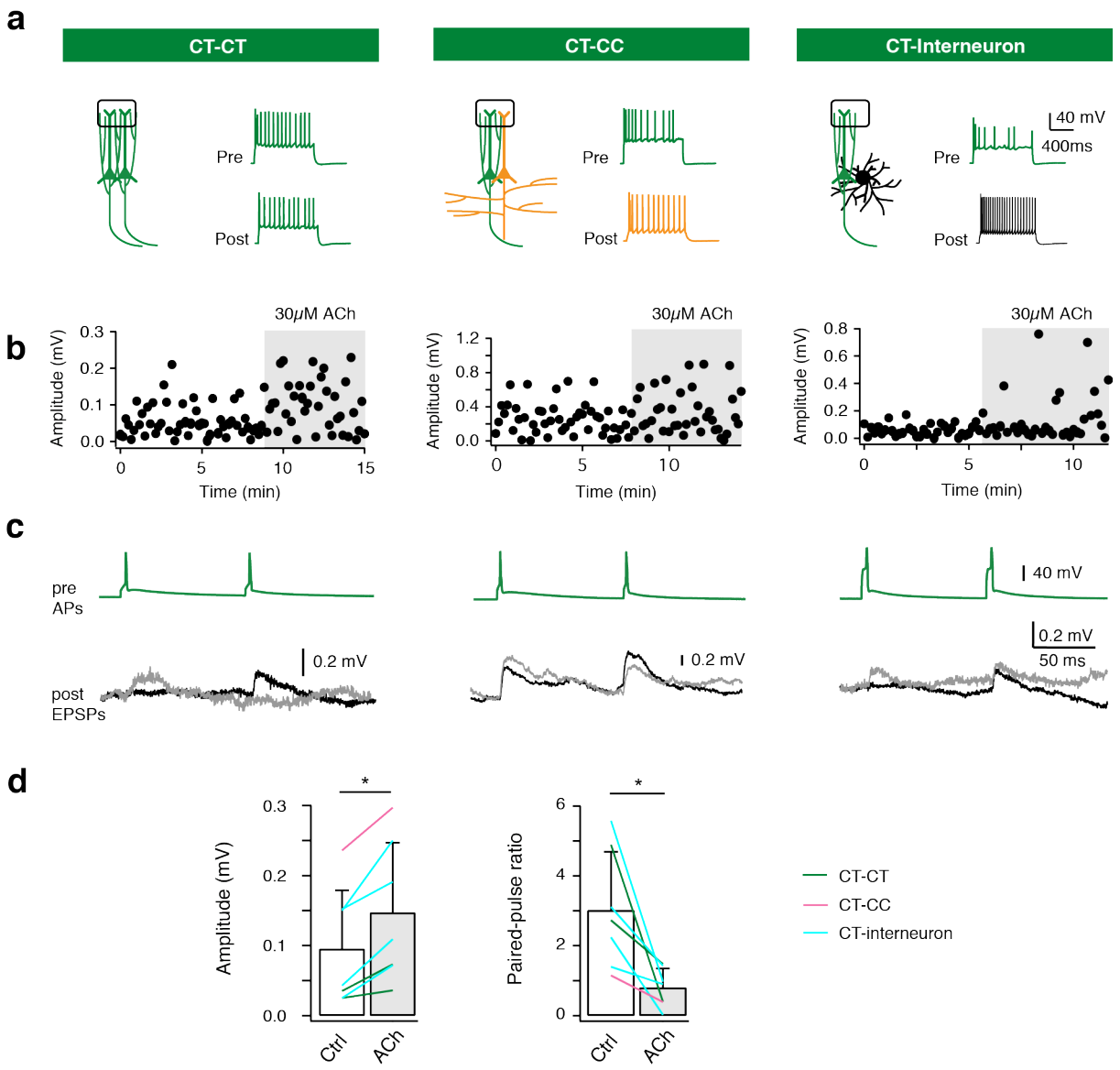

Fig. 7 ACh enhances synaptic efficacy of L6A excitatory connections with a presynaptic CT PC.

(a) Left, schematic representation of the synaptic connections with a presynaptic CT PC. Color code as in Fig. 5. Barrel structures indicate layer 4. Right, corresponding firing patterns of pre- and postsynaptic neurons of the same connection type.

(b) Time course of EPSP amplitude change following bath application of 30 µM ACh in a CT-CT, CT-CC, and CT-interneuron pair.

(c) Overlay of average EPSPs in control (black) and ACh application (gray) phases. Presynaptic APs are shown at the top. Data are recorded from the same pairs as in (b).

(d) Summary data (n = 7) of ACh-induced changes in first uEPSP amplitude and paired-pulse ratio for L6A excitatory pairs with a presynaptic CT L6A PC. Bars indicate the average for each condition; Error bars represent SD. *P < 0.05 for Wilcoxon signed-rank test.

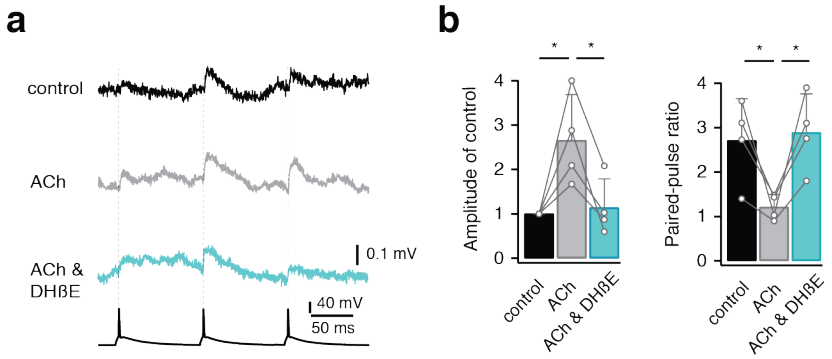

Fig. 8 ACh increases presynaptic release probability of CT PC via activation of $\alpha_4\beta_2$ nAChRs. **(a)** Average EPSPs recorded in control, the presence of ACh (30µM), and of ACh & DHßE (10 µM) from a representative CT-CT connection. Gray phase, bath application of 30µM ACh; Turquoise phase, co-application of ACh and DHßE. The presynaptic APs are shown at the bottom. **(b)** Histograms (n = 4) showing the effect of ACh and DHßE blockade of ACh-induced changes in first uEPSP amplitude and paired-pulse ratio. Data were recorded from L6A synaptic connections with a presynaptic CT PC. Open circles, individual data points; bars, the average for each condition. Error bars represent SD. *P < 0.05 for paired Student's t-test.

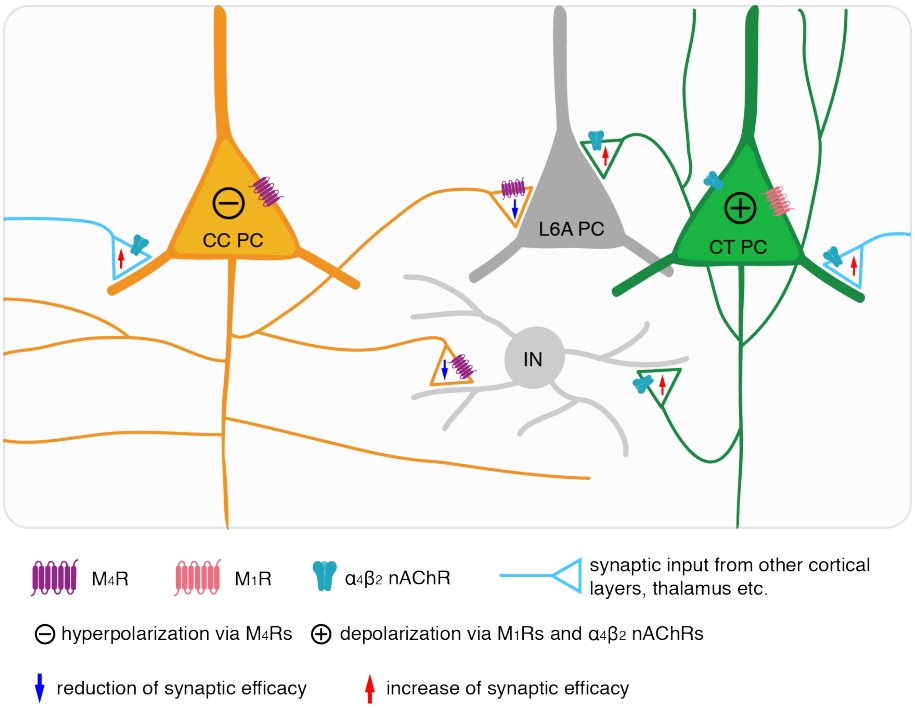

Fig. 9 Cholinergic actions on muscarinic and nicotinic receptors in L6A PCs.

Schematic summary shows cholinergic modulation of L6A microcircuits in rat barrel cortex. ACh affects membrane excitability and presynaptic release probability of L6A PCs via activating muscarinic and/or nicotinic AChRs. Because of the cell type-specific distribution of AChRs at pre- and postsynaptic sites, CC and CT L6A PCs are affected differentially by ACh. The presynaptic CC and CT L6A PC are shown in orange and green, respectively. The postsynaptic L6A PC and interneuron are shown in gray.